Petrological, petrofabric, and oxygen isotopic study of five ungrouped meteorites related to brachinites

Journal Item

Petrological, petrofabric, and oxygen isotopic study of five ungrouped meteorites related to brachinites

Hikari HASEGAWA[1*], Takashi MIKOUCHI[1,2], Akira YAMAGUCHI[3,4], Masahiro YASUTAKE[5], Richard C. GREENWOOD[6], and Ian A. FRANCHI[6]

[1]Department of Earth and Planetary Science, Graduate School of Science, University of Tokyo, Hongo, Bunkyo-ku, Tokyo 113-0033, Japan
[2]The University Museum, The University of Tokyo, Hongo, Bunkyo-ku, Tokyo 113-0033, Japan
[3] Antarctic Meteorite Research Center, National Institute of Polar Research, Tachikawa, Tokyo 190-8518, Japan
[4] Department of Polar Science, School of Multidisciplinary Science, Graduate University for Advanced Sciences, Tachikawa, Tokyo 190-8518, Japan
[5]Division of Earth and Planetary Sciences, Graduate School of Science, Kyoto University, Kyoto 606-8502, Japan
[6]Planetary and Space Sciences, School of Physical Sciences, The Open University, Walton Hall, Milton Keynes MK7 6AA, UK
[*]Corresponding author. E-mail: hasegawah@eps.s.u-tokyo.ac.jp

(Received 21 May 2018; revision accepted 11 December 2018)

Abstract–Northwest Africa (NWA) 6112, Miller Range (MIL) 090206 (+its pairs: MIL 090340 and MIL 090405), and Divnoe are olivine-rich ungrouped achondrites. We investigated and compared their petrography, mineralogy, and olivine fabrics. We additionally measured the oxygen isotopic compositions of NWA 6112. They show similar petrography, mineralogy, and oxygen isotopic compositions and we concluded that these five meteorites are brachinite clan meteorites. We found that NWA 6112 and Divnoe had a *c* axis concentration pattern of olivine fabrics using electron backscattered diffraction (EBSD). NWA 6112 and Divnoe are suggested to have been exposed to magmatic melt flows during their crystallization on their parent body. On the other hand, the three MIL meteorites have *b* axis concentration patterns of olivine fabrics. This indicates that the three MIL meteorites may be cumulates where compaction of olivine grains was dominant. Alternatively, they formed as residues and were exposed to olivine compaction. The presence of two different olivine fabric patterns implies that the parent body(s) of brachinite clan meteorites experienced diverse igneous processes.

INTRODUCTION

Brachinite Clan Meteorites

Brachinites are an ultramafic, dunitic to wherlitic, unbrecciated and essentially unshocked group of meteorites (e.g., Keil 2014). At the time of writing, 44 meteorites are classified as brachinites (cf. Meteoritical Bulletin Database, 2018). In his review of the group, Keil (2014) reported that brachinites are mostly composed of olivine (~71–96 vol%; ~$Fo_{64–73}$), clinopyroxene (minor to ~15 vol%; ~$En_{43–63}Wo_{36–48}$), with variable amounts of plagioclase (0 to ~10 vol%; ~$An_{15–33}$), and minor to trace amounts of orthopyroxene (0 to ~20 vol%; $En_{69–73}Wo_{2–4}$), Fe-sulfides (trace to ~7 vol%), chromite (0 to ~5 vol%), phosphates (0 to ~3 vol%), and metallic Fe-Ni (trace to ~2 vol%). Individual brachinite meteorites have homogeneous mineral compositions and medium- to coarse-grained olivine textures (~0.1–1.5 mm). Preferred orientation and lineation have been noted in some brachinites (e.g., Allan Hills 84025, Elephant Moraine 99402), and olivines in brachinites commonly display triple junctions (e.g, Mittlefehldt et al. 2003). As a consequence of the highly recrystallized rock textures displayed by brachinites, it has been suggested that the group experienced formation under conditions of relatively slow cooling (e.g., Keil 2014). Many researchers have suggested that brachinites may represent partial melt residues, but there is currently no overall consensus concerning the detailed petrogenesis of brachinites (e.g.,

Mittlefehldt et al. 2003; Day et al. 2012; Goodrich et al. 2017).

Furthermore, some researchers pointed out that the definition of brachinites is not well constrained (e.g., Mittlefehldt and McCoy 2014; Goodrich et al. 2017; Greenwood et al. 2017). For example, Northwest Africa (NWA) 6112 is classified as an "ungrouped achondrite" because the Fo composition ($Fo_{75–72}$) of olivine is slightly outside the range of brachinites ($Fo_{70–65}$) and similar to those of the ungrouped achondrite, Divnoe ($Fo_{80–72}$) (cf. Meteoritical Bulletin Database, 2018). On the other hand, NWA 7605 has a similar olivine composition to NWA 6112, but is classified as a brachinite, despite of its high Fo composition ($Fo_{73.9–73.8}$) (cf. Meteoritical Bulletin Database, 2018). Brachinites are now classified by using a variety of characteristics (e.g., petrology, mineralogy, whole-rock chemical compositions and oxygen isotopic compositions). Several researchers have drawn attention to the similarities of some meteorites to brachinites (e.g., Nehru et al. 2003; Day et al. 2012; Gardner-Vandy et al. 2013; Goodrich et al. 2017). Day et al. (2012) defined these related meteorites as "brachinite-like achondrites." Although there is currently no consensus concerning a set of criteria for defining brachinites, Goodrich et al. (2017) classified brachinites and those achondrites showing some similarities to brachinites into four groups, i.e., (1) Brachinites, (2) Brachinite-like achondrites, (3) Ungrouped achondrites with similarities to brachinites, and (4) Other achondrites classified as brachinites but for which no detailed studies have been done. They collectively called the meteorites of these four groups "brachinite clan" meteorites.

A variety of unresolved questions remain concerning the origin of brachinites. It has been suggested that there is a lack of olivine-rich achondrites representing mantle materials from early-formed differentiated planetesimals, the so-called "Great Dunite Shortage" (Greenwood et al. 2015). If brachinites are from a variety of distinct parent bodies, then they may, at least in part, account for the apparent scarcity of olivine-rich achondrites (Greenwood et al. 2017). This raises the question as to the nature of the environment in which the brachinites and brachinite-like meteorites formed and in particular whether they actually represent mantle-derived asteroidal materials? In order to better constrain the conditions that prevailed during and after crystallization on brachinite parent body(s?), we have undertaken a study of their olivine fabrics (e.g., Hasegawa et al. 2016). The presence of a preferred orientation and lineation within brachinites provides essential information about their formation history, but so far has only been the subject of a few studies (e.g., Mittlefehldt et al. 2003). Consequently, we focus here on such textures in brachinites and related meteorites and discuss the implications of these petrofabrics for the formational environment of this important group of meteorites.

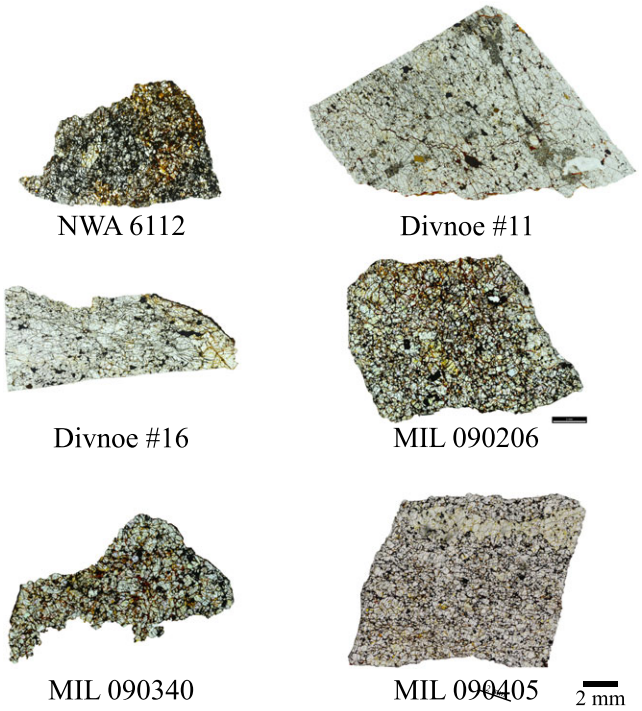

Fig. 1. Optical photomicrographs (open nicol) of the samples. The scale bar is 2 mm. (a) NWA 6112, (b) Divnoe #11, (c) Divnoe #16, (d) MIL 090206, (e) MIL 090340, and (f) MIL 090405.

SAMPLES

This study was undertaken on five ungrouped achondrites: NWA 6112, Divnoe, Miller Range (MIL) 090206, MIL 090340, and MIL 090405, which has been suggested may be related to the brachinites (Petaev et al. 1994; Goodrich et al. 2012; Corder et al. 2014; Goodrich et al. 2017; Meteoritical Bulletin Database, 2018). NWA 6112 is a 1040 g rock partially covered by fusion crust, found in Morocco in 2000 (Meteoritical Bulletin Database, 2018). NWA 6112 is suggested to be related to Divnoe only on Meteoritical Bulletin Database, and has no previous study. A thin section and two rock fragments were prepared from a rock chip of NWA 6112 for this study (Fig. 1). The two fragments were used to determine the oxygen isotopic composition of NWA 6112.

Divnoe is a meteorite that was found in September 1981 in Stavropol province, Russia (Graham 1983). In this study, we prepared two thin sections of Divnoe from the same rock chip and examined them (Fig. 1).

MIL 090206, 090340, 090356, 090405, 090805, and 090963 are US Antarctic meteorites that are thought to be pieces of a single meteorite fall, based on their very similar and unique mineralogical compositions and their discovery by the meteorite expedition in the same season (Antarctic Meteorite Newsletter, 2012). Welten et al. (2014) suggested that the similar ^{10}Be and ^{26}Al concentrations as well as similar chemical compositions in MIL 090206, 090340, and 090963 confirmed their pairing. MIL 090206, MIL 090340, and MIL 090405 are ~17, 4.7, and 58.8 g rocks, respectively (Antarctic Meteorite Newsletter, 2011). These meteorites were originally classified as ureilites (Antarctic Meteorite Newsletter, 2011). However, Goodrich et al. (2012) and Warren and Rubin (2012) pointed out that these MIL meteorites should have been classified as brachinites and not as ureilites based on their mineralogy and petrology. We studied thin sections of MIL 090206 (MIL 090206, 11), 090340 (MIL 090340, 10), and 090405 (MIL 090405, 9) that were supplied by the Meteorite Working Group. There are some previous studies on MIL 090206, 090340, and 090405, but is no previous report on the thin sections which we examine (Goodrich et al. 2012, 2017; Warren and Rubin 2012; Singerling et al. 2013; Corder et al. 2014; Welten et al. 2014). These three samples are the largest samples among these six MIL meteorites (Figs. 1d–f).

ANALYTICAL METHODS

Electron Probe Micro Analyzer

We performed quantitative analysis and X-ray elementary mapping of the thin sections of the samples using Electron Probe Micro Analyzer (EPMA)—JEOL JXA-8900L and Field Emission Electron Probe Micro Analyzer (FE-EPMA)—JEOL JXA-8530F with wavelength dispersive X-ray spectroscopes (WDS), to clarify assemblage textures of various mineral phases with different chemical compositions. The accelerating voltage was 15 kV and the beam current for X-ray mapping was 120 nA. For quantitative analysis, the beam current was 30 nA (accelerating voltage: 20 kV) for olivine, 12 nA for other silicates, and 20 nA for metal, and the spot sizes were 2 μm in diameter. We used natural and synthetic minerals and metals for standards whose compositions have been by determined by wet chemical techniques. The analyzed elements are Si, Al, Ti, Fe, Mg, Ca, Na, K, Cr, Ni, P, and S in X-ray mapping. Si, Al, Ti, Fe, Mn, Mg, Ca, Na, Cr, and Ni were analyzed for olivine, and K was additionally analyzed for other silicates in quantitative analysis. For metal in quantitative analysis, Si, S, Fe, Ni, Co, Zn, Cu, Cr, and P were measured. Counting times at peak wavelengths were 10 s and those at background on both sides of the peak wavelengths were 5 s. In particular, 100 s at peak wavelength and 50 s at background were applied for olivine measurements. The chemical compositions from quantitative analysis were calculated by the ZAF correction method.

Field Emission Gun Scanning Electron Microscope

Polished thin sections were observed by Field Emission Gun Scanning Electron Microscope (FEG-SEM)—JEOL JSM-7100F equipped with energy-dispersive X-ray spectroscopy (EDS) at the National Institute of Polar Research (NIPR) in secondary electron image (SEI) and backscattered electron image (BEI) modes. The accelerating voltage was 15 kV and the beam current was in the range of 1–2 nA.

Electron Backscatter Diffraction

Processes to form igneous and metamorphic rocks involve some combination of crystal growth, solution, movement, and deformation, which is expressed as changes in texture or microstructure (e.g., Higgins 2006). Meteorites, particularly achondrites, are igneous and metamorphic rocks and contain the information of their thermal history in their textures, mineral assemblages, and fabrics. Fabrics (grain orientations) in rocks have been used mainly to establish flow directions and mechanisms in lava flow and dykes. Criteria of fabric are based on the orientations of the grain shapes. It is commonly called shape preferred orientations (SPO). The grains that define the fabric of rocks can generally be crystals, clasts, or enclaves. Therefore, the fabric can be determined by the orientations of the crystal lattices, known as lattice preferred orientations (LPO) or crystallographic preferred orientations (CPO).

To give a quantitative rating to the apparent SPO, we analyzed CPO of olivine crystals by electron backscatter diffraction (EBSD). We employed the JEOL JSM-7100F at NIPR equipped with an EBSD detector (AZtec Energy, Oxford Instruments). The collection semi-angle of the EBSD detector was about 37.5°. The analyzed samples were tilted by approximately 70° from the horizontal. The analyses were conducted at 15 kV accelerating voltage, 10 nA beam current, and 25 mm working distance. Information on the phase and crystal orientation can be solved by analyzing obtained diffraction patterns. In this approach, we can perform analysis of crystal structure on small submicron area. As the sample surface is required to be in the best condition for EBSD analysis, it is necessary to perform final polishing with colloidal silica after polishing with a 1/4 micron diamond paste. The stage was moved

manually and systematically to different sites (each roughly 5 × 7 mm^2 in size) on each sample. All EBSD patterns of olivine were automatically indexed using AZtec software. In this software, there is only *Pnma* (a = 10.2 Å, b = 6.0 Å, c = 4.8 Å) space group data of *International Tables for Crystallography* to index olivine structure, but *Pbnm* (a = 4.8 Å, b = 10.2 Å, c = 6.0 Å) is normally used as the olivine space group. In this paper, we discuss olivine's space group as *Pbnm*. Therefore, we exchanged crystallographic axes as b axis (*Pbnm*) = a axis (*Pnma*), c axis (*Pbnm*) = b axis (*Pnma*), and a axis (*Pbnm*) = c axis (*Pnma*). Only those indexed with a mean angular deviation (MAD) <1.0° were accepted and recorded. Any ambiguous indexing was immediately verified using energy-dispersive X-ray (EDX) spectroscopy before being accepted or rejected. In each PTS, one point was analyzed for each olivine crystal and the results were plotted as stereographic projections of upper-hemisphere, equal-area plots according to the main olivine crystallographic axes [100] (a axis), [010] (b axis), and [001] (c axis). The pole figures were contoured by mean uniform density distribution (MUD) with half width 10 and cluster size 5. Misorientation distribution graphs showing the M-index, which was defined by Skemer et al. (2005), quantify the strength of the fabric recorded in each case (Fig. 3). They defined the misorientation index (M-index) as the difference between the observed distribution of uncorrelated misorientation angles and the distribution of uncorrelated misorientation angles for a random fabric. The magnitude of M-index increases with fabric strength from 0 (random fabric) to 1 (single crystal fabric).

Laser Fluorination Analysis

Oxygen isotopic analysis of NWA 6112 was undertaken at the Open University using an infrared laser fluorination system (Miller et al. 1999). The normal operating procedure involves loading ~2 mg aliquots of samples and standards into a Ni sample block containing 22 drilled wells. The sample block is then loaded into a two-part chamber, made vacuum tight using a compression seal with a copper gasket and quick-release KFX clamp (Miller et al. 1999). A 3 mm thick BaF_2 window at the top of the chamber allows simultaneous viewing and laser heating of samples.

Following sample loading the cell was heated under vacuum for a minimum of 24 hours and to a temperature of at least 70 °C to remove most of the adsorbed atmospheric moisture. Prior to fluorination, any remaining atmospheric moisture was removed by flushing the chamber with aliquots of BrF_5, such that the final blank was less than 60 nmol O_2. Sample heating in the presence of BrF_5 was carried out using an integrated 50W infrared CO_2 laser (10.6 μm) and video system mounted on an X-Y-Z gantry supplied by Photon Machines Inc. (Greenwood et al. 2017). After fluorination, the released O_2 was purified by passing it through two cryogenic (liquid nitrogen) traps and over a bed of heated KBr. The isotopic composition of the purified oxygen was analyzed using a Thermo Fisher MAT 253 dual inlet mass spectrometer (mass resolving power 200). Interference at m/z = 33 by NF^+ was monitored by performing scans for $NF_2{}^+$ on the sample gas before analyzing each sample; this was below interference levels during all sample analyses reported here. Our current system precision based on repeat analyses (N = 39) of our obsidian internal standard is: ±0.052‰ for $\delta^{17}O$; ±0.094‰ for $\delta^{18}O$; and ±0.017‰ for $\Delta^{17}O$ (2σ) (Starkey et al. 2016). Oxygen isotopic analyses are reported in standard δ notation, where $\delta^{18}O$ has been calculated as: $\delta^{18}O = [(^{18}O/^{16}O_{sample}/^{18}O/^{16}O_{ref}) - 1] \times 1000$ (‰) and, similarly, for $\delta^{17}O$ using the $^{17}O/^{16}O$ ratio. $\Delta^{17}O$, which represents the deviation from the terrestrial fractionation line, has been calculated using the linearized format of Miller (2002): $\Delta^{17}O = 1000 \ln(1 + \delta^{17}O/1000) - \lambda 1000 \ln(1 + \delta^{18}O/1000)$, $\lambda = 0.5247$, and was determined using 47 terrestrial whole-rock and mineral separate samples (Miller et al. 1999; Miller 2002).

RESULTS

Petrography and Mineralogy

NWA 6112

The thin section of NWA 6112 shows a dark appearance (Fig. 1). Brownish or yellowish veins, which are thought to be the result of the terrestrial weathering, are observed at the grain boundaries and also along cracks in olivine grains. The polished thin section (PTS) shows granoblastic and poikilitic textures. Most of the PTS consists of coarse-grained olivine grains (size: ~1.5 mm). Other major constituent minerals are clinopyroxene and plagioclase. The olivine grains have rectilinear boundaries which frame triple junctions. The shock degree is weak as seen from only weak wavy extinction in olivine grains. The grain size of clinopyroxene is diverse (~0.2–1.5 mm) and the largest one is 0.8 × 1.4 mm in size. The clinopyroxene grains are anhedral and poikilitically contain rounded olivine chadacrysts. Clinopyroxene shows a lamellar texture under optical microscopic observation. Plagioclase is also anhedral and has variable grain size (~0.1–1 mm). Both clinopyroxene and plagioclase are surrounded by olivine grains. Other minor component minerals are chromite, troilite, orthopyroxene, Fe-Ni metal, phosphate, Fe-oxides, and/or -hydroxides. Chromite exists as fine-grained (<50 μm) inclusions in olivine grains. Troilite grains are also fine-grained (<50 μm) but are present

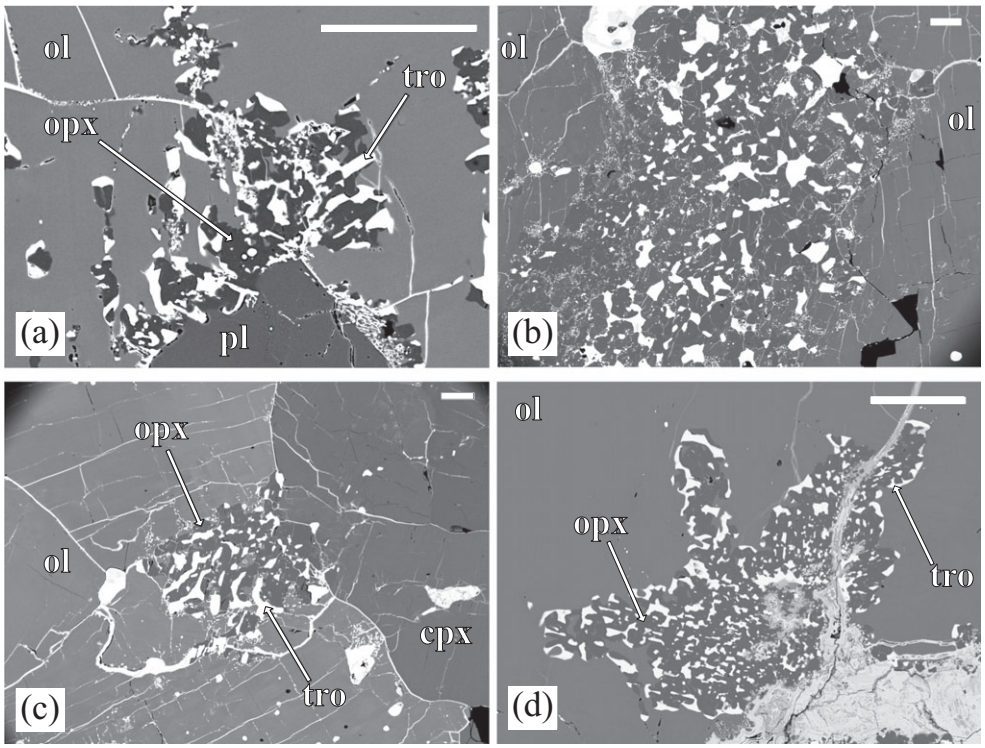

Fig. 2. Backscattered electron (BSE) images of fine-grained assemblage of troilite (tro) and orthopyroxene (opx). All the scale bars which are located at the right top are 50 μm. In all figures, white lines (cracks) are filled with Fe-oxides or -hydroxides, probably deposit by terrestrial weathering. (a) NWA 6112. (b) Divnoe #11. The fine-grained area is "opaque-rich lithology" described by Petaev et al. (1994). (c) MIL 090206. The single large opx grain exists on the right edge. (d) MIL 090340. The gray area at the right bottom is Fe-oxides or -hydroxides, probably deposit by terrestrial weathering.

interstitially to olivine grains. At the grain boundaries and cracks, fine-grained (size: <10 μm) assemblages of orthopyroxene and troilite are present (Fig. 2a). Fe-Ni metal is observed as rounded inclusions (size: <10 μm) in olivine grains and most of them are associated with troilite.

The coarse-grained olivine has a small compositional range (e.g., $Fo_{\sim 75-72}$) (Table 1). In Mg map, chemical zoning of olivine is observed in the PTS. However, normal core-to rim zoning is not observed in each grain, but chemical zoning overlaps several grains. The compositions of clinopyroxene are $En_{46.1}Wo_{43.3}$ (Table 2). At the mineral grain boundaries or along cracks, the composition of orthopyroxene is $En_{75.6}Wo_{1.7}$ (Table 3). Troilite has ~38 wt% sulfur and ~60 wt% Fe. Fe-Ni metal contains ~3.5 wt% Ni. Plagioclase has the composition of $An_{\sim 21.2}$ and chromite has Al_2O_3: ~8 wt%, FeO: ~28 wt% and Cr_2O_3: ~57 wt% (Table 4).

Divnoe

We observed and analyzed two PTSs (#11 and #16) of Divnoe (Fig. 1). The PTSs are partially surrounded by brownish or blackish weathering crust and several veins are also brown or yellow. Both PTSs show granoblastic and poikilitic textures. Both PTSs largely consist of coarse mineral grains which were described as "coarse-grained lithology" in Petaev et al. (1994). In PTS #11, we found the presence of fine-grained textures which were described as "dark lithology" in Zaslavskaya and Petaev (1990) or "opaque-rich lithology" in Petaev et al. (1994). These slight differences of textures and modal abundances in the two PTSs probably reflect the inhomogeneous texture of Divnoe as reported by previous studies (e.g., Zaslavskaya and Petaev 1990). Coarse-grained areas are mainly composed of olivine. Other constituent minerals are clinopyroxene, orthopyroxene, chromite, Fe-Ni metal, Fe-sulfide, Fe-oxides, and/or -hydroxides. Petaev et al. (1994) reported the existence of plagioclase in Divnoe, but we could not find any in the two PTSs that we studied. The absence of plagioclase in two PTSs comes from the inhomogeneity of Divnoe reported in the previous studies (e.g., Zaslavskaya and Petaev 1990). Olivine grains are coarse (grain size: ~2 mm) and mostly have elongated shapes. Most of olivine grains contain tiny rounded inclusions (grain size: up to ~30 μm) composed of Fe-Ni metal and Fe-sulfide. The elongated olivine crystals display SPO in both PTSs. The degree of shock metamorphism is weak to moderate as seen from undulatory extinction of

Table 1. Representative compositions of olivine in NWA 6112, Divnoe, MIL 090206, MIL 090340, and MIL 090405.

	NWA 6112		Divnoe		MIL 090206		MIL 090340		MIL 090405	
	Avg.	SD	Avg.	SD	Avg.	SD	Avg.	SD	Avg.	SD
SiO_2	37.4	0.2	37.5	0.1	37.5	0.2	37.1	0.2	37.2	0.1
Al_2O_3	b.d.		b.d.		b.d.		b.d.		b.d.	
TiO_2	b.d.		b.d.		b.d.		b.d.		b.d.	
FeO	23.9	0.3	24.1	0.2	24.6	0.3	25.7	0.6	24.7	0.2
MnO	0.50	0.01	0.47	0.01	0.49	0.01	0.48	0.02	0.47	0.01
MgO	38.9	0.2	38.6	0.2	38.1	0.3	37.3	0.4	38.3	0.2
CaO	0.08	0.01	0.02	0.00	0.08	0.01	0.08	0.01	0.06	0.01
Na_2O	b.d.		b.d.		b.d.		b.d.		b.d.	
Cr_2O_3	0.03	0.00	b.d.		0.04	0.01	0.03	0.01	0.03	0.00
NiO	b.d.		b.d.		b.d.		b.d.		b.d.	
Total	100.8	0.4	100.7	0.3	100.8	0.3	100.7	0.4	100.8	0.3
N	39		64		58		84		47	
#Fo	74.3	0.3	74.1	0.2	73.4	0.3	72.0	0.6	73.4	0.2

Table 2. Representative compositions of clinopyroxene in NWA 6112, Divnoe, MIL 090206, MIL 090340, and MIL 090405.

			Divnoe									
	NWA 6112		Coarse-grained		Exolution		MIL 090206		MIL 090340		MIL 090405	
	Ave.	SD	Ave.	SD	Ave.	SD	Ave.	SD	Ave.	SD	Ave.	SD
SiO_2	54.1	0.3	53.9	0.4	53.8	0.4	53.8	0.3	53.2	0.4	53.8	0.2
Al_2O_3	0.41	0.07	0.94	0.06	0.60	0.05	0.69	0.06	0.75	0.03	0.68	0.07
TiO_2	0.24	0.04	0.17	0.03	0.14	0.06	0.25	0.04	0.26	0.03	0.28	0.04
FeO	6.48	0.3	6.14	0.2	5.81	0.3	6.3	0.2	6.2	0.1	6.4	0.2
MnO	0.22	0.04	0.24	0.06	0.20	0.06	0.19	0.05	0.2	0.03	0.22	0.06
MgO	15.8	0.1	16.3	0.2	16.3	0.3	16.0	0.1	16.8	0.2	16.1	0.1
CaO	20.7	0.4	20.6	0.3	22.2	0.2	21.1	0.3	21.2	0.3	20.9	0.3
Na_2O	0.46	0.06	0.42	0.06	0.32	0.05	0.52	0.07	0.41	0.04	0.54	0.06
Cr_2O_3	0.74	0.07	0.79	0.06	0.58	0.05	0.78	0.07	0.73	0.03	0.82	0.07
NiO	0.02	0.01	b.d.		0.03	0.01	0.03	0.02	0.03	0.02	b.d.	
Total	99.2	0.3	99.5	0.4	100	0.3	99.7	0.3	99.8	0.4	99.7	0.2
N	63		48		21		36		37		51	
En	46.1	0.4	47.1	0.3	45.9	0.4	46.1	0.3	47.3	0.2	46.4	0.4
Fs	10.6	0.3	10.0	0.2	9.2	0.4	10.2	0.3	9.8	0.4	10.4	0.3
Wo	43.3	0.5	43.0	0.3	45.0	0.3	43.7	0.5	42.9	0.5	43.2	0.5

olivine. Clinopyroxene has an anhedral shape and the grain sizes range widely from ~0.1 to 1.5 mm. Rounded inclusions of metal and sulfide are also observed in clinopyroxene grains. Orthopyroxene grains are very large and their maximum diameters are ~1–6 mm. Orthopyroxene have lamellar textures (width: ~10 μm) composed of clinopyroxene (inverted pigeonite) and surround anhedral olivine grains (grain size: ~0.5–1.5 mm) and rounded olivine grains (grain size: ~0.1–0.5 mm). Chromite, Fe-Ni metal, and Fe-sulfide grains are also present in orthopyroxene grains. Chromite is anhedral and ranges from ~50 μm to ~1 mm in size. Some of chromite grains exist at the edge of orthopyroxene and others are interstitially enclosed by olivine grains. Fe-Ni metal grains (size: ~0.2–0.5 mm) have anhedral shapes and are adjacent to olivine and orthopyroxene. Most of them have the rims of Fe-oxides and/or -hydroxides and some of them are almost completely Fe-oxides or -hydroxides, probably because of the terrestrial weathering. Troilite is present as small grains (size: <~0.2 mm) but two large elongated grains (size: ~0.4 × 1.1 and 0.2 × 0.9 mm) are characteristically observed in PTS #11. As a whole, the grain boundaries are filled with Fe-oxides and/or -hydroxides. Fine-grained areas are composed of troilite (~0.1 mm in size), Fe-Ni metal (~20–30 μm in size), and orthopyroxene (~30 μm in size) (Fig. 2b). These observations are basically consistent with earlier studies (e.g., Petaev et al. 1994).

Table 3. Representative compositions of orthopyroxene in NWA 6112, Divnoe, MIL 090206, MIL 090340, and MIL 090405.

			Divnoe				MIL 090206				MIL 090340		MIL 090405			
	NWA 6112		Fine-grained		Exolution		Oikocryst		Fine-grained		Fine-grained		Poikilitic		Fine-grained	
	Ave.	SD	Ave.	SD	Ave.	SD	Ave.	SD	Ave.	SD	Ave.	SD	Ave.	SD	Ave.	SD
SiO_2	55.5	0.4	55.7	0.5	54.4	0.2	54.4	0.5	53.2	0.6	54.0	0.5	55.2	0.3	54.7	0.6
Al_2O_3	0.12	0.06	0.11	0.05	0.41	0.06	0.26	0.03	0.10	0.03	0.05	0.02	0.25	0.03	0.01	0.03
TiO_2	0.05	0.05	0.04	0.04	0.12	0.03	0.10	0.01	0.05	0.02	0.05	0.02	0.12	0.01	0.02	0.02
FeO	15.02	0.2	13.6	0.3	16.1	0.2	16.8	0.4	15.5	0.3	15.7	0.3	16.8	0.2	16.1	0.3
MnO	0.45	0.06	0.44	0.07	0.47	0.06	0.45	0.02	0.40	0.02	0.38	0.03	0.41	0.03	0.50	0.02
MgO	28.1	0.3	29.1	0.2	26.6	0.3	26.8	0.3	31.4	0.5	30.9	0.4	26.8	0.4	28.0	0.5
CaO	0.89	0.3	0.53	0.1	1.12	0.3	1.2	0.02	0.71	0.02	0.48	0.02	1.2	0.02	0.71	0.02
Na_2O	b.d.		b.d.		b.d.		b.d.		b.d		b.d.		b.d.		b.d.	
Cr_2O_3	0.14	0.07	0.05	0.07	0.23	0.05	0.25	0.03	0.13	0.01	0.08	0.01	0.19	0.02	0.09	0.01
NiO	0.05	0.01	0.04	0.01	0.03	0.02	b.d.		b.d.		b.d.		b.d.		b.d.	
Total	100.3	0.4	99.7	0.3	99.5	0.2	100.3	0.3	100.7	0.6	100.8	0.5	100.9	0.3	100.1	0.6
N	37		34		24		49		25		28		26		24	
En	75.6	0.3	78.4	0.2	73.1	0.4	72.3	0.3	77.3	0.2	77.1	0.2	72.3	0.3	74.5	0.2
Fs	22.7	0.4	20.6	0.4	24.7	0.3	25.4	0.4	21.4	0.3	22.0	0.3	25.4	0.3	24.1	0.2
Wo	1.7	0.4	1.0	0.5	2.2	0.5	2.3	0.3	1.3	0.3	0.9	0.3	2.2	0.4	1.4	0.3

Table 4. Representative compositions of orthopyroxene in NWA 6112, Divnoe, and MIL 090206.

	NWA 6112		Divnoe		MIL 090206	
	Ave.	SD	Ave.	SD	Ave.	SD
SiO_2	63.8	0.4	59.8		64.1	1.1
Al_2O_3	22.5	0.2	26.29		22.7	0.3
TiO_2	b.d.		n.d.			
FeO	0.25	0.55	0.02		0.33	0.95
MnO	b.d.		n.d.		0.03	0.02
MgO	b.d.		0.01		0.03	0.02
CaO	4.3	0.1	7.5		3.66	0.08
Na_2O	8.6	0.1	6.99		9.17	0.09
K_2O	0.44	0.04	0.09		0.57	0.05
Cr_2O_3	b.d.		0.01			
V_2O_3	b.d.					
NiO	b.d.					
P_2O_5	b.d.		n.d.			
Total	99.9	0.3	101.1		100.6	
N	107		47		158	
An	21.2	0.6	37.02		17.5	0.3
Or	2.6	0.2	0.54		3.3	0.3
Ref.	This study		Petaev et al. (1994)		Goodrich et al. (2017)	

Results show that the chemical composition of olivine in "coarse-grained lithology" is fairly heterogeneous, but individual grains do not display clear zoning patterns. The composition of clinopyroxene, another coarse-grained mineral, is $En_{47.1}Wo_{43.0}$ (Table 2). Inverted pigeonite is composed of an orthopyroxene host ($En_{73.1}Wo_{2.2}$) and exsolved augite ($En_{45.9}Wo_{45.0}$) (Tables 2 and 3). The exsolved clinopyroxene is more magnesian and contains less calcium than that of the "coarse-grained lithology." Orthopyroxene in the "opaque-rich lithology" has the composition of $En_{78.4}Wo_{1.0,}$ which is more magnesian and poor in calcium relative to that of in the "coarse-grained lithology" (Table 3). While we did not find any plagioclase grains, Petaev et al. (1994) reported that the An# of plagioclase was 37.02 (Table 4). Chromite has Al_2O_3: ~10 wt%, FeO: ~27 wt%, and Cr_2O_3: ~56 wt%. Troilite contains 36.2 wt% S and Fe-Ni metal contains 7.0 wt% Ni.

MIL 090206/090340/090405

We initially studied PTSs of MIL 090206/090340/090405 (hereafter MILs) by optical microscopy (Fig. 1). Brownish veins, which represent terrestrial weathering products, run along cracks and mineral grain boundaries in all the PTSs.

MIL 090206 is modally dominated by olivine, in the PTS studied here, and other constituent minerals are orthopyroxene, chromite, clinopyroxene, troilite, Fe-Ni metal, Fe-oxides, and -hydroxides. We did not detect plagioclase grains in this PTS, although Goodrich et al. (2017) reported the existence of plagioclase in MIL 090206. Olivine shows a large grain size variation (0.1–1 mm in size). Large grains show elongated shapes and lineation. Orthopyroxene exists as a large oikocryst grain (~2 × 6 mm in size) and contains rounded chadacrysts of olivine, chromite, troilite, and Fe-Ni metal. The chadacrysts of olivine and chromite are a few hundred microns in size and those of troilite and Fe-Ni metal are less than 0.1 mm in size. Chromite is

also present as anhedral coarse grains (0.2–1 mm in size) interstitial to olivine grains. Clinopyroxene is anhedral small grains (<0.2 mm in size). Troilite and Fe-Ni metal are present as anhedral small grains (<0.1 mm in size) at the mineral boundaries. At the grain boundaries and cracks, fine-grained assemblages composed of orthopyroxene, troilite, and Fe-Ni metal (each mineral phase: <10 μm in size) exist (Fig. 2c). Fe-oxides and -hydroxides are also common at the mineral boundaries and cracks.

MIL 090340 is mostly composed of olivine. Other components are clinopyroxene, chromite, troilite, Fe-Ni metal, orthopyroxene, Fe-oxides, and -hydroxides. The size of olivine ranges 0.1–1.5 mm. Large grains show elongated shapes, but a lineation is not obvious. Clinopyroxene forms small, anhedral grains (~0.5 mm in size). Chromite is present as both fine- and coarse-grained crystals (<50 μm and 0.2–1 mm in size). Coarse-grained chromite is anhedral and interstitial to olivine grains. Fine-grained chromite has a rounded shape and is enclosed by olivine grains. Troilite and Fe-Ni metal are present as anhedral small grains (<0.2 mm in size) along mineral boundaries. Along grain boundaries and cracks, fine-grained assemblages composed of orthopyroxene, troilite, and Fe-Ni metal (each mineral phase: <10 μm in size) are present (Fig. 2d). Orthopyroxene was not detected except for these assemblages as Goodrich et al. (2017) reported, although Warren and Rubin (2012) described orthopyroxene in MIL 090340. Fe-oxides and -hydroxides are also common at the mineral boundaries and cracks.

MIL 090405 is also mostly composed of olivine. Other constituent minerals are clinopyroxene, chromite, orthopyroxene, troilite, Fe-Ni metal, Fe-oxides, and -hydroxides. Some olivine grains are up to 1.5 mm in diameter, but smaller grains down to 0.1 mm are also present. Large grains show elongated shapes and a clear lineation. Clinopyroxene exists as a large oikocryst grain (~2 × 8 mm in size) and contains rounded chadacrysts of olivine, orthopyroxene, troilite, and Fe-Ni metal. The size of chadacrysts of olivine and orthopyroxene ranges from 0.2 mm to 0.8 mm and troilite and Fe-Ni metal are under 0.1 mm in size. Clinopyroxene is also present as anhedral grains (<0.5 mm in size) interstitial to olivine grains. Chromite was also detected as anhedral coarse grains (a few hundred microns in size) interstitial to olivine. Troilite and Fe-Ni metal are present as anhedral small grains (<0.1 mm in size) along mineral boundaries. At grain boundaries and cracks, there are fine-grained assemblages composed of orthopyroxene, troilite, and Fe-Ni metal (each mineral phase: <10 μm in size). Fe-oxides and -hydroxides are also common along mineral boundaries and cracks.

Thus, the similar textures and mineral compositions of the three MIL meteorites support the pairing of these meteorites (Welten et al. 2014). Since the mineral compositions of the three MILs are identical, hereafter we describe the representative mineral compositions of the three MIL meteorites.

X-ray maps show complicated patterns of chemical zoning in coarse-grained olivine grains. Olivine compositions vary from $Fo_{\sim 74}$ to $Fo_{\sim 70}$ (Table 1). In some olivine grains, we found reverse zoning of Fe-Mg, but other olivine grains did not show clear patterns of chemical zoning. This is consistent with the observations of Warren and Rubin (2012). The Ca content of olivine does not vary between coarse-grained ones and chadacrysts (~0.06–0.08 wt% CaO). Minor minerals are clinopyroxene, chromite, orthopyroxene, Fe-Ni metal, and Fe-sulfide. Clinopyroxene grains are homogeneous ($En_{\sim 46.1–47.3}Wo_{\sim 42.9–43.7}$) and enclose chadacrysts of olivine ($Fo_{\sim 72–73.4}$) and orthopyroxene ($En_{\sim 72.3}Wo_{\sim 2.3}$) (Table 1,2,3). The composition of these olivine chadacrysts is similar to the core composition of coarse-grained olivine showing Fe-Mg reverse zoning. At the boundaries of olivine–olivine, olivine–chromite, and within olivine, we found fine-grained orthopyroxene ($En_{\sim 74.5–77.3}Wo_{\sim 0.9–1.4}$), troilite (S: ~38 wt%), and Fe-Ni metal (Ni: ~4 wt%) (Table 3).

Olivine Grain Petrofabrics

Clear lineation (SPO) textures were found for Divnoe, MIL 090206, and MIL 090405 by the optical microscopic observations. In these meteorites, most of olivine grains are elongated and the direction of the longer dimension appears preferentially oriented.

NWA 6112 shows the CPO pattern which has the concentration of [001] (*c* axis) (Fig. 3). Both [100] (*a* axis) and [010] (*b* axis) of olivine in NWA 6112 plot as broad girdles normal to [001] (*c* axis).

For NWA 6112, a total of 123 crystallographic measurements of olivine were collected, which yield a fabric strength of $M = 0.16$.

For Divnoe #11, a total of 171 crystallographic measurements of olivine were collected, which yield a fabric strength of $M = 0.25$. [001] (*c* axis) plots as point maxima within the apparent lineation. [100] (*a* axis) and [010] (*b* axis) both plot as broad girdles normal to [001] (*c* axis). In an analogous way, Divnoe #16 shows the same CPO pattern which has the concentration of [001] (*c* axis) (Fig. 3). For Divnoe #16, a total of 124 crystallographic measurements of olivine were collected, which yield a fabric strength of $M = 0.24$. The CPO pattern with *c* axis concentration was also reported in Ando et al. (2003).

Unlike NWA 6112 and Divnoe, MILs show the CPO pattern which has the concentration of [010] (*b* axis) (Figs. 4d–f). [010] (*b* axis) plots as point maxima normal to the direction of the observed lineation on the PTS. [001]

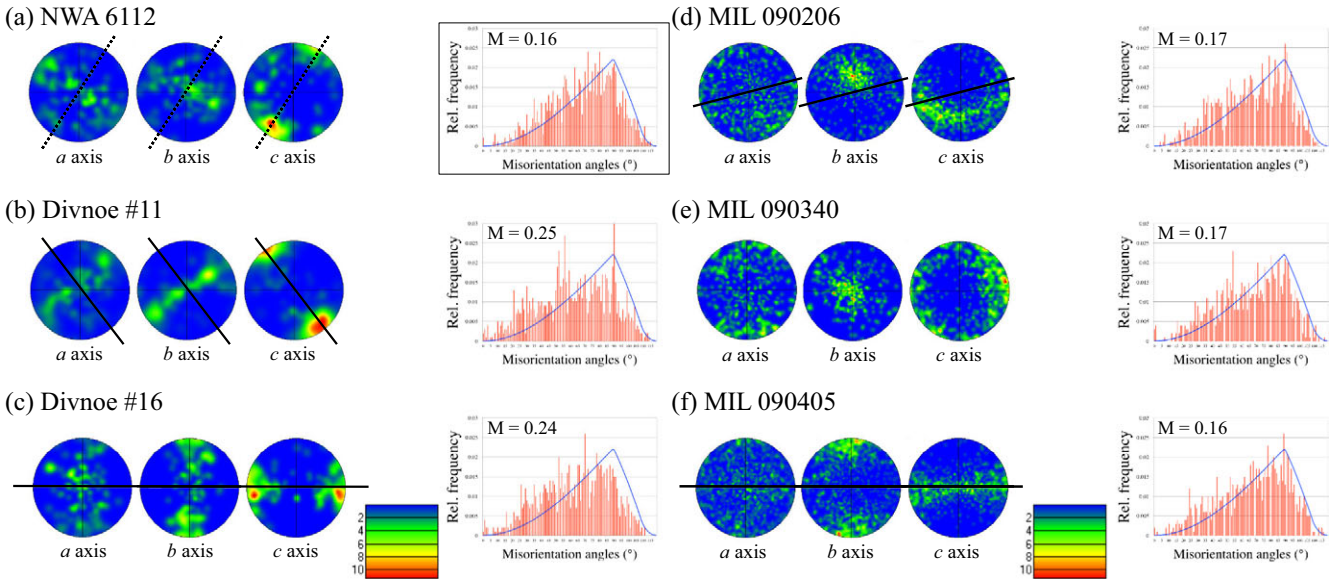

Fig. 3. Results of EBSD analyses of (a) NWA 6112, (b) Divnoe #11, (c) Divnoe #16, (d) MIL 090206, (e) MIL 090340, and (f) MIL 090405. The data are displayed as stereographic, equal-area, upper-hemisphere projections. Contour plots show the measured crystallographic orientations of olivine crystals of each sample according to the [100] (*a* axis), [010] (*b* axis), and [001] (*c* axis) as mean uniform density distributions (mud). Solid black line denotes the presumed lineation and dotted line shows the presumed weak lineation. On MIL 090340, no obvious lineation is observed. Fabric strengths are quantified by the M-Index (Skemer et al. 2005). The right graphs show the distributions of misorientation angles for the samples. The blue lines on the graphs are the theoretical curves for a random fabric.

(*c* axis) plots as broad girdles parallel to the lineation and [100] (*a* axis) does not show clear patterns. For MIL 090206, a total of 355 crystallographic measurements of olivine were collected, which yield a fabric strength of $M = 0.17$. For MIL 090340, a total of 223 crystallographic measurements of olivine were collected, which yield a fabric strength of $M = 0.17$. MIL 090340 displays the same trend of crystallographic orientation as is seen in MIL 090206. The convergence of [010] (*b* axis) and the girdle of [001] (*c* axis) were detected. In the same manner, for MIL 090405, a total of 545 crystallographic measurements of olivine were collected, which yield a fabric strength of $M = 0.16$. [010] (*b* axis) concentrates on one direction and [001] (*c* axis) plots on a girdle normal to the [010] (*b* axis). [100] (*a* axis) does not show an obvious concentration of crystallographic orientations.

Oxygen Isotopic Compositions

Duplicate analysis of NWA 6112 gave the following mean oxygen isotopic composition: $\delta^{17}O$, 2.34 ± 0.00‰ (1σ); $\delta^{18}O$, 4.89 ± 0.01‰ (1σ); and $\Delta^{17}O$, −0.23 ± 0.01‰ (1σ). The oxygen isotope analysis of NWA 6112 plots close to that of both Divnoe (Greenwood et al. 2012) and MIL 090340 (Goodrich et al. 2012) (Fig. 4). All three meteorites plot within the oxygen isotope field of brachinites defined by Greenwood et al. (2012) and close to a number of other brachinite-like achondrites (Greenwood et al. 2017) (Fig. 4).

DISCUSSION

Comparison of General Petrography

All of the PTSs of NWA 6112, Divnoe #11, #16, MIL 090206, 090340, and 090405 show coarse-grained igneous textures and are mostly composed of olivine. Other constituent minerals are clinopyroxene, orthopyroxene, plagioclase, troilite, Fe-Ni metal, Fe-oxides, and -hydroxides. We found plagioclase only in NWA 6112, but previous studies have reported the presence of plagioclase in Divnoe and MIL 090206 (e.g., Petaev et al. 1994; Goodrich et al. 2017). NWA 6112, Divnoe, and MILs have essentially the same mineral assemblage, which is more or less identical to that of the brachinites (e.g., Keil 2014). The grain size of olivine is variable in each PTS. The size of olivine grain in all the PTSs ranges from 0.1 mm to 2 mm. Divnoe has coarser olivine grains (0.5–2 mm in size) than the other samples (0.1–1.5 mm in size). A common feature of these meteorites is that the larger olivine grains in a PTS display elongated shapes. Olivine crystals commonly display SPO and have boundaries which generally meet at triple junctions. Preferred orientation and lineation of olivine was previously

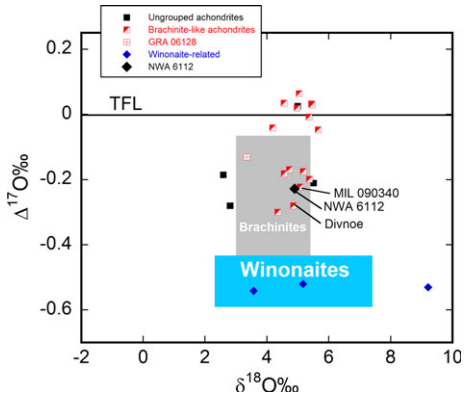

Fig. 4. Oxygen isotopic composition of NWA 6112 shown in relation to the field of brachinites (gray box), as defined by Greenwood et al. (2012, 2017), various brachinite-like achondrites (see Greenwood et al. 2017 for references), and winonaites (blue box) (Greenwood et al. 2012, 2017). NWA 6112 plots close to both Divnoe (Greenwood et al. 2012) and MIL 090340 (Goodrich et al. 2012).

reported from three brachinites: Allan Hills (ALH) 84025, Elephant Moraine (EET) 99402, and EET 99407 (these EET meteorites are paired) (Mittlefehldt et al. 2003). In this study, we found that Divnoe, MIL 090206, and MIL 090405 display clear olivine grain lineation and NWA 6112 shows weak lineation. Characteristically, elongate olivine grains in MILs show cracks normal to the direction of elongation. This may indicate that MILs experienced stress from the direction normal to the lineation direction.

The dark appearance of NWA 6112 and MILs might be taken to indicate a similarity with ureilites (Goodrich et al. 2012; Warren and Rubin 2012), as in fact MILs were initially misclassified as ureilites. However, in contrast to ureilites, NWA 6112 and MILs do not contain a carbon-rich matrix. Instead of a carbon-rich matrix, these meteorites display an assemblage consisting of orthopyroxene and opaque minerals (troilite and Fe-Ni metal), which is also found in several brachinites and makes the PTS appear black under the optical microscope (e.g., Goodrich et al. 2011, 2017). Another notable signature is that NWA 6112, Divnoe, and MILs contain large augite oikocrysts. In particular, the size of augite grains in NWA 6112 and MIL 090405 exceeds 1 cm. The augite grains poikilitically enclose chadacrysts of olivine and orthopyroxene. This mineralogical evidence, combined with the results of oxygen isotope analysis (Fig. 4), suggests that these five meteorites belong to brachinite clan.

Comparison of Mineral Chemistry

Olivine is the most abundant phase in NWA 6112, Divnoe, MILs, and the brachinites. In a review paper by Keil (2014), the range of olivine compositions in brachinites is ~$Fo_{73–64}$. In the samples we studied, MILs have $Fo_{\sim 72–73.4}$ olivine which is within the range of brachinites, but NWA 6112 ($Fo_{\sim 74.3}$) and Divnoe ($Fo_{\sim 74.1}$) are slightly out of the range. The minor element compositions of olivine in NWA 6112, Divnoe, and MILs are within the range of brachinites. In general, olivine in brachinites is more ferroan than those in any other group of achondrites (Goodrich et al. 2011). The CaO content of olivine in brachinites is ~0.08–0.3 wt%, and is higher than acapulcoites, lodranites, and winonaites but is lower than ureilites (Fig. 5) (Goodrich et al. 2011). Most ureilites are known to be a partial melt residue quenched rapidly from high (~1200 °C), super-solidus temperatures (e.g., Singletary and Grove 2003). The relatively high CaO content in NWA 6112 and MILs may indicate that these meteorites experienced higher temperature and more rapid cooling than acapulcoites, lodranites, and winonaites. The Cr_2O_3 content of olivine in NWA 6112, Divnoe, and MILs is very low (<~0.03 wt%). Similar low abundance of Cr is also found in brachinites (Keil 2014). On the other hand, olivines in ureilites display much higher Cr_2O_3 contents (>0.3 wt%). These differences confirm that NWA 6112 is not related to ureilites.

In NWA 6112, Divnoe, and MILs, clinopyroxene is coarse-grained. The composition of clinopyroxene is within the range of brachinites (~$En_{40–63}Wo_{36–48}$) (Keil 2014), with all the samples studied showing very similar compositional ranges (Fig. 6). In contrast, the compositions of orthopyroxene in NWA 6112, Divnoe, and MILs are not uniform. (Fig. 6). In these meteorites, orthopyroxene is a part of the assemblage which consists of orthopyroxene, Fe-sulfide, and metal. Characteristically, in MILs, large clinopyroxene grains poikilitically enclose orthopyroxene. The fine-grained orthopyroxene is more Fe-rich than the coarse-grained one, possibly because secondary fluorescence from troilite/metal could have caused. Among these five meteorites, the orthopyroxene composition of Divnoe is the highest in Mg content. In Divnoe, inverted pigeonites were also observed. We use these compositions to apply the two-pyroxene thermometer of Nakamuta et al. (2017). The estimated temperatures are ~930 ± 15 °C from orthopyroxene and ~820 ± 20 °C from augite. These differences suggest that the equilibration between the lamellae and the host pyroxene was not achieved. This result is consistent with Petaev et al. (1994). We also calculated the temperature for MILs and obtained ~930 ± 20 °C from orthopyroxene and ~880 ± 30 °C from augite, respectively. This is consistent with Goodrich et al. (2017).

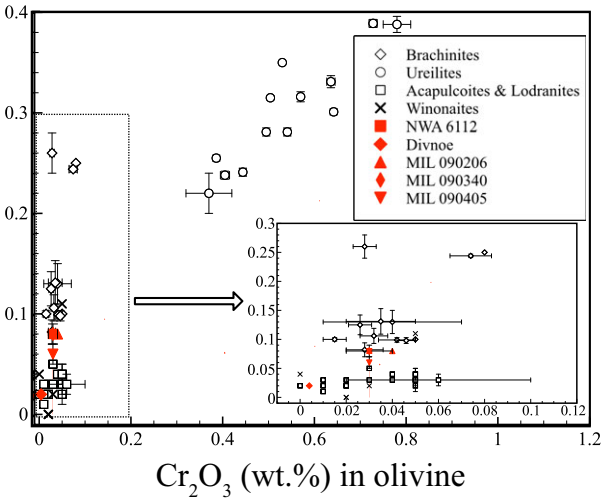

Fig. 5. CaO and Cr_2O_3 contents of olivine in NWA 6112, Divnoe, MILs, and various achondrites. The enlarged view of brachinite range is shown on the lower right. Sources of data are as follows. Brachinites: Johnson et al. (1977), Warren and Kallemeyn (1989), Goodrich and Righter (2000), Mittlefehldt et al. (2003), Goodrich et al. (2011), Day et al. (2015). Ureilites: Goodrich et al. (2011). Acapulcoites + Lodranites: Nagahara (1992), Takeda et al. (1994), Papike et al. (1995), Mittlefehldt et al. (1996), Folco et al. (2006), Burroni and Folco (2008).

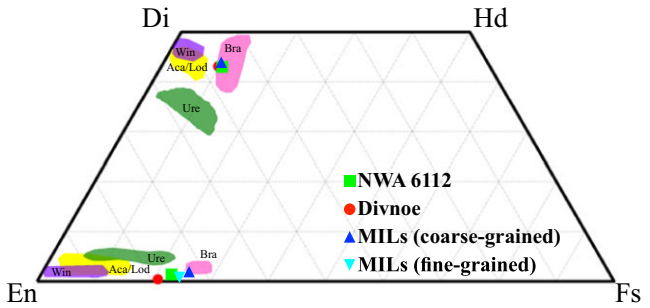

Fig. 6. Pyroxene quadrilateral showing compositions of clinopyroxene and orthopyroxene in NWA 6112, Divnoe, MILs, and various achondrites. The composition ranges of achondrites (Bra = brachinites; Ure = ureilites; Aca/Lod = acapulcoites + lodranites; Win = winonaites) are modified after fig. 7 in Goodrich et al. (2011).

Plagioclase was found only in NWA 6112 in this study, although the presence of plagioclase was reported in Divnoe and MIL 090206 (Petaev et al. 1994; Goodrich et al. 2017). Divnoe has a higher anorthite component ($An_{\sim 37}$) compared to NWA 6112 ($An_{\sim 21}$) and MIL 090206 ($An_{\sim 18}$). Keil (2014) reported that the anorthite component of plagioclase in brachinites is $An_{\sim 15–33}$. On the one hand, Goodrich et al. (2011) described more anorthite-rich range of $An_{\sim 22–40}$. However, plagioclase in achondrites has various compositions. The composition of plagioclase in acapulcoites and lodranites ranges $An_{\sim 6–31}$ (Nagahara and Ozawa 1986; Nagahara 1992; Takeda et al. 1994; Mittlefehldt et al. 1996; McCoy et al. 1997; Folco et al. 2006; Burroni and Folco 2008) and that in winonaites ranges $An_{\sim 9–25}$ (Kimura et al., 1992). Therefore, we cannot say NWA 6112, Divnoe, and MIL meteorites are brachinites based on only plagioclase composition, but these compositions are all within the range of brachinites.

NWA 6112, Divnoe, and MILs also contain chromite, Fe-sulfide, and metal. Chromite is generally coarse-grained (~0.5–1 mm in size). The compositions of chromite in NWA 6112, Divnoe, and MILs are very similar to those of brachinites. We also calculated the equilibration temperatures for NWA 6112, Divnoe, and MILs using the olivine-spinel thermometer of Wlotzka (2005). The temperatures we obtained are ~830 °C for Divnoe, ~860 °C for NWA 6112, and ~910 °C for MILs. These temperatures are similar to those obtained in previous studies of brachinites, with the notable exception of Brachina, for which a higher equilibration temperatures of ~1000–1100 °C have been reported (e.g., Petaev et al. 1994; Goodrich et al. 2017).

Fe-sulfide and Fe-Ni metal are present as a fine-grained assemblage associated with orthopyroxene. This assemblage is also common in brachinites (Goodrich et al. 2011, 2017). This assemblage is similar to the reduction rims and veins found in olivine of ureilites and makes grain boundary darkening, which leads it a compelling resemblance to ureilites in transmitted light. However, Goodrich et al. (2017) described the significant differences between the assemblage in brachinites and the reduction rims in ureilites. As they reported, we also found olivine grains with slight reverse chemical zoning ($Fo_{72–74}$) in MIL meteorites. This zoning in olivine might be associated with the formation of this assemblage, although this assemblage shows high degree of terrestrial weathering. In Divnoe, NWA 6112, and MILs, the assemblage is composed of orthopyroxene, troilite, and Fe-Ni metal. These constituent phases might not be primary, because this assemblage was weathered on the Earth. Goodrich et al. (2017) discussed two possibilities of the primary phases (orthopyroxene + troilite or orthopyroxene + Fe-Ni metal). Their and our observations suggest that the primary phases are orthopyroxene + troilite. If so, this assemblage originated from interaction of primary olivine with introduced S-rich vapors via reactions such as those discussed by Singerling et al. (2013), Colson (1992), Norman et al. (1995), and Shearer et al. (2012), as Goodrich et al. (2017) suggested. Based on mineralogical data obtained in this study, it is clear that

NWA 6112 is a member of the brachinite clan along with both Divnoe and MILs.

Olivine Petrofabrics

Both NWA 6112 and Divnoe clearly show the same CPO patterns. Olivine grains in both NWA 6112 and Divnoe are preferentially aligned along [001] (*c* axis), whereas [100] (*a* axis) and [010] (*b* axis) are randomly oriented. The CPO pattern that *c* axis of olivine is preferentially oriented has been reported in EET 99407 and ALH 84025 brachinites (Mittlefehldt et al. 2003) as well as in Divnoe (Ando et al. 2003). Mittlefehldt et al. (2003) suggested that EET 99407 and ALH 84025 are igneous, specifically cumulate rocks, based on four principal observations. (1) Quantitatively confirmed olivine lineations and probable lineations; (2) the consistency of specific olivine orientation patterns with those of previously measured cumulates; (3) the relative strength of olivine-preferred orientations; and (4) the absence of internal strain systems produced by solid-state flow. Moreover, the *c* axis concentration is also found in ureilite (Dingo Pup Donga) and shergottite (ALH 77005) (Berkley et al. 1980; Berkley and Keil 1981). Berkley and Keil (1981) suggested that ALH 77005 was formed as a cumulate rock while in the act of magmatic flow. In addition, Nagahara and Ozawa (1986) reported the *c* axis concentration of olivine in Yamato-791493 (lodranite) and indicated the existence of a strong magmatic laminar flow parallel to the direction of the elongation of olivine crystals at the time of its formation. Therefore, it seems likely that NWA 6112 and Divnoe experienced similar formation processes to EET 99407, ALH 84025 (brachinite), Dingo Pup Donga (ureilite), ALH 77005 (Martian meteorite), and Yamato-791493 (lodranite). Thus, we conclude that NWA 6112 and Divnoe were exposed to magmatic melt flows during their crystallization (Fig. 7a).

MIL 090206, 090340, and 090405 have the comparable CPO patterns. However, unlike the above samples, the olivine grains in MIL 090206, 090340, and 090405 are preferentially aligned along [010] (*b* axis). The direction of the *b* axis concentration and the lineation bisect each other at right angles. On the other hand, the dimension of [001] (*c* axis) is arranged on a plane but [100] (*a* axis) does not show clear patterns. The *b* axis concentration patterns of olivine in MILs are similar to those observed by Brothers (1964) in the Rum and Skaergaad cumulate complexes. This suggests that the CPO patterns of olivine in MILs were formed during accumulation at the bottom of a magma chamber or in a thick lava flow. A similar pattern of olivine CPO has also been reported in a wehrlitic intrusion of Oman ophiolites (Boudier 1991). Boudier (1991) described the CPO generally related to axial compression stresses such as undergone by cumulate rocks (Fig. 7b). However, a similar pattern can also be produced in other compaction-related environments where post-crystallization axial compression deforms the crystal lattice by activation of the relevant olivine slip system, similarly aligning the shortest axis parallel to the direction of compaction, yet allowing the other two axes to be arranged radially within the lineation (Fig. 7c) (Holtzman et al. 2003). This indicates that the MILs may be formed as residues and experienced compaction after crystallization on the parent body.

Parent Bodies of Brachinite Clan Meteorites

The oxygen isotopic compositions of NWA 6112, Divnoe, and MILs are all within the range of brachinites as defined by Greenwood et al. (2012, 2017) (Fig. 4). In particular, Divnoe ($\delta^{18}O = 4.86$, $\Delta^{17}O = -0.28$) has nearly identical compositions to ALH 84025 ($\delta^{18}O = 4.89 \pm 0.17$, $\Delta^{17}O = -0.30 \pm 0.01$) (Greenwood et al. 2012). NWA 6112 and MIL 090206 have virtually identical $\Delta^{17}O$ values. These oxygen isotopic compositions are clearly distinguished from other achondrites (e.g., acapulcoites, lodranites, and winonaites) (Greenwood et al. 2012). However, the CPO patterns of olivine in MILs are different from those of NWA 6112 and Divnoe. They have the CPO patterns that are preferentially aligned along [010] (*b* axis), whereas [100] (*a* axis) and [001] (*c* axis) are randomly oriented. It suggests that the formation processes of MILs, NWA 6112, and Divnoe are somewhat different in spite of their mineralogical similarities.

Greenwood et al. (2017) separated brachinite clan meteorites into two groups ("brachinites and brachinite-related meteorites" and "Mg-rich, brachinite-like") on the basis of olivine Mg-Fe composition. According to the criterion of this, MILs belong to "brachinites and brachinite-related meteorites." On the other hand, Divnoe and NWA 6112 are indicated to be "Mg-rich, brachinite-like." This grouping corresponds to the two different olivine CPO patterns. It is suggested that there was a magma chamber and melt flow on the parent body of "Mg-rich, brachinite-like." This means "Mg-rich, brachinite-like" meteorites are not "primitive" achondrites but differentiated meteorites and their formation process is different from that of Brachina. Moreover, MILs belonging to "brachinites and brachinite-related meteorites" also show the olivine CPO which was suggested to have been formed by accumulation or compaction. This indicates that there are several meteorites which experienced different degree of melting (partial melting to complete melting) in brachinite clan meteorites.

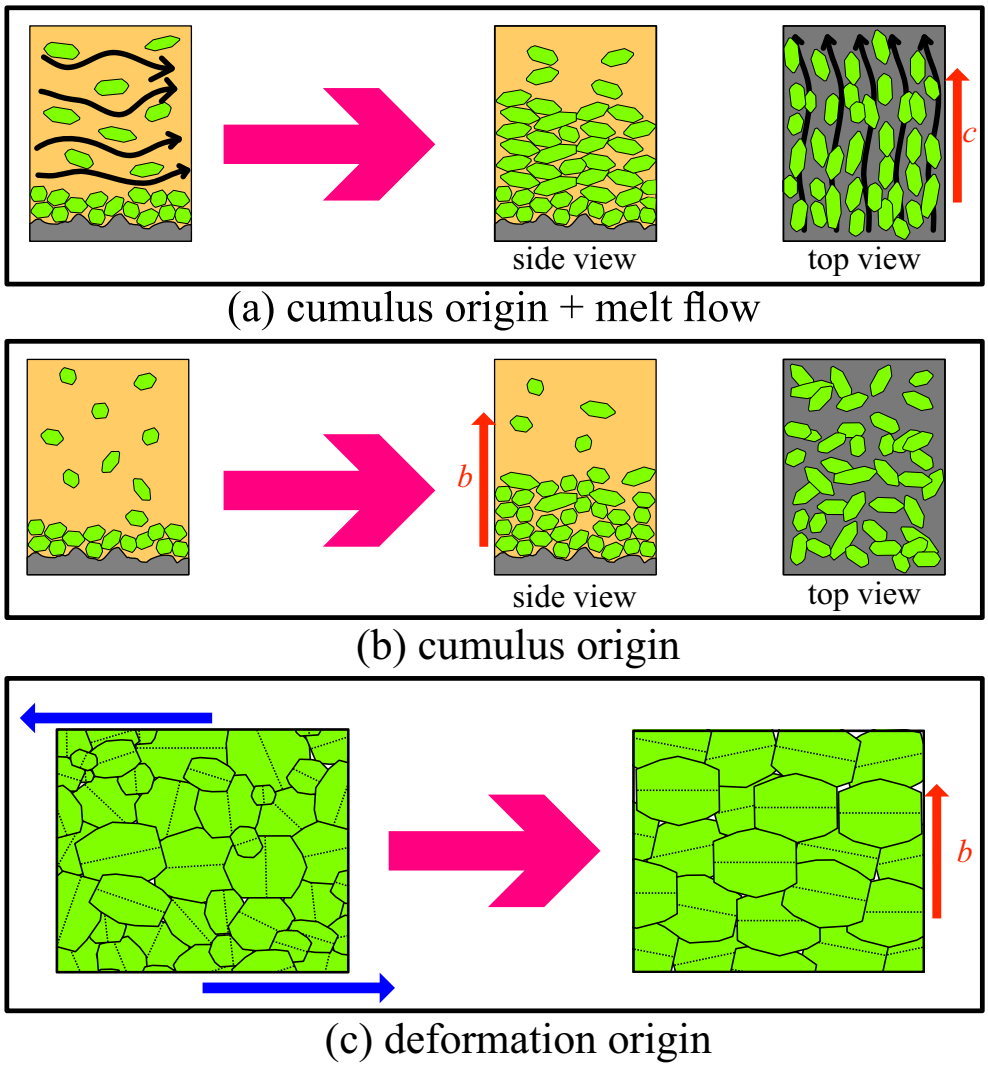

Fig. 7. Schematic illustrations of the three processes forming different olivine CPO patterns. a) Accumulation exposed to a magmatic flow that forms *c* axis concentration. b) Accumulation that forms *b* axis concentration. c) compaction-related environment where post-crystallization axial compression deforms the crystal lattice by activation of the relevant olivine slip system, similarly aligning the shortest axis (*b* axis) parallel to the direction of compaction, yet allowing the other two axes to be arranged radially within the lineation.

From another point of view, the parent body of NWA 6112 and MILs is suggested to be the same because of their identical oxygen isotopic compositions. If NWA 6112 and MILs came from the same parent body, their parent body was heterogeneous enough to make two different olivine CPO patterns. On that parent body, it is suggested that there are several magma chambers and some of them had magmatic convection to make a *c* axis concentration pattern. Neumann et al. (2018) indicated that the final global interior structure of acapulcoite-lodranite parent body consisted of differentiated (iron core, silicate mantle), partially differentiated, and undifferentiated layers by their model calculations. If this interior structure was analog to the brachinite parent body, the samples in this study came from the silicate mantle or partially differentiated layer in the brachinite parent body. This suggests that the formation process of brachinite was not simple.

CONCLUSIONS

In this study, we observed and analyzed the PTSs of NWA 6112, Divnoe, MIL 090206, MIL 090340, and MIL 090405. These meteorites are known to have similarities to brachinites. Therefore, we compared these meteorites to each other and to some other meteorite groups. Based on the results of this study, we come to the following conclusions:

1. NWA 6112, an ungrouped achondrite which has not been previously studied, has a similar petrography and mineral composition to Divnoe, MIL 090206, MIL 090340, MIL 090405, and the brachinite clan meteorites.
2. NWA 6112 and Divnoe display comparable CPO patterns of olivine, such that [001] (*c* axis) plots as point maxima within the apparent lineation. [100] (*a* axis) and [010] (*b* axis) both plot as broad girdles normal to [001] (*c* axis). Therefore, NWA 6112 and Divnoe were probably exposed to magmatic melt flow during their crystallization.
3. MIL 090206, MIL 090340, and MIL 090405 show the CPO patterns of olivine such that [010] (*b* axis) plots as point maxima normal to the direction of the observed lineation on the PTS. This indicates that MIL 090206, MIL 090340, and MIL 090405 may be cumulates where compaction of olivine grains was dominant. Alternatively, they formed as residues and were exposed to olivine compaction.
4. NWA 6112, Divnoe, MIL 090206, MIL 090340, and MIL 090405 have similar mineral and oxygen isotopic compositions, but the CPO patterns of olivine crystal are different. This means there were multiple formation conditions among brachinite clan meteorites. These correspond to their different parent bodies or to the different regions on the single parent body. The parent body(s) of brachinite clan meteorites was suggested to be differentiated as concluded by Mittlefehldt et al. (2003).

Acknowledgments—We thank the US Meteorite Working Group for the loan of MIL samples and Bruno Fectay and Carine Bidaut for providing the NWA 6112 sample. Discussions with Drs. J. Ando and N. Tomioka are greatly appreciated. We also thank NIPR (National Institute of Polar Research, Ms. T. Ojima) for supporting SEM and EBSD works. Mr. H. Yoshida and Mr. K. Ichimura supported electron microprobe works at Department of Earth and Planetary Science, University of Tokyo. This work was supported by a Grant-in-Aid for JSPS Fellowship to HH (16J03702). We thank Dr. D. W. Mittlefehldt and two anonymous reviewers for helpful reviews, and Dr. C. A. Goodrich for editorial handling.

Editorial Handling—Dr. Cyrena Goodrich

REFERENCES

Ando J., Tomioka N., Petaev M. L., Kanagawa K., Honda K., Shibata Y., and Yamanaka S. 2003. Microstructures of olivine in the weakly shocked divnoe meteorite. American Geophysical Union, Fall Meeting 2003, abstract id.V31D-0972.

Berkley J. L. and Keil K. 1981. Olivine orientation in the ALHA77005 achondrite. *American Mineralogist* 66:1233–1236.

Berkley J. L., Taylor G. J., Keil K., Harlow G. E., and Prinz M. 1980. The nature and origin of ureilites. *Geochimica et Cosmochimica Acta* 44:1579–1597.

Boudier F. 1991. Olivine xenocrysts in picritic magmas. *Contributions to Mineralogy and Petrology* 109:114–123.

Brothers R. N. 1964. Petrofabric analyses of Rhum and Skaergaard layered rocks. *Journal of Petrology* 5:255–274.

Burroni A. and Folco L. 2008. Frontier Mountain meteorite specimens of the acapulcoite-lodranite clan: Petrography, pairing, and parent-rock lithology of an unusual intrusive rock. *Meteoritics & Planetary Science* 43:731–744.

Colson R. O. 1992. Mineralization on the Moon? Theoretical considerations of Apollo 16 "rusty rocks," sulfide replacement in 67016, and surface-correlated volatiles on lunar volcanic glass. Proceedings, 22nd Lunar and Planetary Science Conference. pp. 427–436.

Corder C. A., Day J. M. D., RumbleIII D., Assayag N., Cartigny P., and Taylor L. A. 2014. Petrology and geochemistry of achondrites LEW 88763, MIL 090206 and MIL 090405: Comparisons with acapulcoite-lodranites, brachinites and chondrites (abstract #2752). 45th Lunar and Planetary Science Conference. CD-ROM.

Day J. M. D., Walker R. J., Ash R. D., Liu Y., Rumble D. III, Irving A. J., Goodrich C. A., Tait K., McDonough W. F., and Taylor L. A. 2012. Origin of felsic achondrites Graves Nunataks 06128 and 06129, and ultramafic brachinites and brachinite-like achondrites by partial melting of volatile-rich primitive parent bodies. *Geochimica et Cosmochimica Acta* 81:94–128.

Day J. M. D., Corder C. A., Rumble D. III, Assayag N., Cartigny P., and Taylor L. A. 2015. Differentiation processes in FeO-rich asteroids revealed by the achondrite Lewis Cliff 88763. *Meteoritics & Planetary Science* 50:1750–1766.

Folco L., D'Orazio M., and Burroni A. 2006. Frontier Mountain 93001: A coarse-grained, enstatite-augite-oligoclase-rich, igneous rock from the acapulcoite-lodranite parent asteroid. *Meteoritics & Planetary Science* 41:1183–1198.

Gardner-Vandy K. G., Lauretta D. S., and McCoy T. J. 2013. A petrologic, thermodynamic and experimental study of brachinites: Partial melt residues of an R chondrite-like precursor. *Geochimica et Cosmochimica Acta* 122:36–57.

Goodrich C. A. and Righter K. 2000. Petrology of unique achondrite Queen Alexandra Range 93148: A piece of the pallasite (howardite-eucrite-diogenite?) parent body? *Meteoritics & Planetary Science* 35:521–535.

Goodrich C. A., Kita N. T., Spicuzza M. J., Valley J. W., Zipfel J., Mikouchi T., and Miyamoto M. 2011. The Northwest Africa 1500 meteorite: Not a ureilite, maybe a brachinite. *Meteoritics & Planetary Science* 45:1906–1928.

Goodrich C. A., Kita N. T., and Warren P. H. 2012. MIL 090340 and MIL 090206: Two more brachinite-like achondrites mis-identified as ureilites (abstract #5272). 75th Annual Meeting of the Meteoritical Society.

Goodrich C. A., Kita N. T., Sutton S. R., Wirick S., and Gross J. 2017. The Miller Range 090340 and 090206 meteorites: Identification of new brachinite-like achondrites with implications for the diversity and petrogenesis of the brachinite clan. *Meteoritics & Planetary Science* 52:949–978.

Graham A. L. 1983. Meteoritical Bulletin, No. 61. *Meteoritics* 18:257–258.

Greenwood R. C., Franchi I. A., and Gibson J. M. 2012. Oxygen isotope variation in achondrites: The influence of primordial, asteroidal and terrestrial processes. *Geochimica et Cosmochimica Acta* 94:146–163.

Greenwood R. C., Barrat J.-A., Scott E. R. D., Haack H., Buchanan P. C., Franchi I. A., Yamaguchi A., Johnson D., Bevan A. W. R., and Burbine T. H. 2015. Geochemistry and oxygen isotope composition of main-group pallasites and olivine-rich clasts in mesosiderites: Implications for the "Great Dunite Shortage" and HED-mesosiderite connection. *Geochimica et Cosmochimica Acta* 169:115–136.

Greenwood R. C., Burbine T. H., Miller M. F., and Franchi I. A. 2017. Melting and differentiation of early-formed asteroids: The perspective from high precision oxygen isotope studies. *Chemie der Erde—Geochemistry* 77:1–43.

Hasegawa H., Mikouchi T., and Yamaguchi A. 2016. Mineralogical and petrofabric study of brachinite-like meteorites Miller Range 090206, 090340 and 090405 (abstract #2131). 47th Lunar and Planetary Science Conference. CD-ROM.

Higgins M. 2006. *Quantitative textural measurements in igneous and metamorphic petrology*. Cambridge: Cambridge University Press. https://doi.org/10.1017/CBO9780511535574.

Holtzman B. K., Kohlstedt D. L., Zimmerman M. E., Heidelbach F., Hiraga T., and Hustoft J. 2003. Melt segregation and strain partitioning: Implications for seismic anisotropy and mantle flow. *Science* 301:1227–1230.

Johnson J. E., Scrymgour J. M., Jarosewich E., and Mason B. 1977. Brachina meteorite—A chassignite from South Australia. *Records of the South Australian Museum* 17:309–319.

Keil K. 2014. Brachinite meteorites: Partial melt residues from an FeO-rich asteroid. *Chemie der Erde—Geochemistry* 74:311–329.

McBride K., Harrington R., Satterwhite C., Corrigan C., and Welzenbach L. 2011. Antarctic Meteorite Newsletter. *Antarctic Meteorite Newsletter* 34:1–29.

McCoy T. J., Keil K., Clayton R. N., Mayeda T. K., Bogard D. D., Garrison D. H., and Wieler R. 1997. A petrologic and isotopic study of lodranites: Evidence for early formation as partial melt residues from heterogeneous precursors. *Geochimica et Cosmochimica Acta* 61:623–637.

Miller M. F. 2002. Isotopic fractionation and the quantification of 17 O anomalies in the oxygen three-isotope system: An appraisal and geochemical significance. *Geochimica et Cosmochimica Acta* 66:1881–1889.

Miller M. F., Franchi I. A., Sexton A. S., and Pillinger C. T. 1999. High precision $\delta^{17}O$ isotope measurements of oxygen from silicates and other oxides: Method and applications. *Rapid Communications in Mass Spectrometry* 13:1211–1217.

Mittlefehldt D. W. and McCoy T. J. 2014. Achondrites and irons: Products of magmatism on strongly heated asteroids. In *35 seasons of US Antarctic meteorites (1976–2010): A pictorial guide to the collection*, edited by Righter K., Corrigan C., McCoy T. and Harvey R. Hoboken, New Jersey: John Wiley & Sons. pp. 79–99.

Mittlefehldt D. W., Lindstrom M. M., Bogard D. D., Garrison D. H., and Field S. W. 1996. Acapulco- and Lodran-like achondrites: Petrology, geochemistry, chronology, and origin. *Geochimica et Cosmochimica Acta* 60:867–882.

Mittlefehldt D. W., Bogard D. D., Berkley J. L., and Garrison D. H. 2003. Brachinites: Igneous rocks from a differentiated asteroid. *Meteoritics & Planetary Science* 38:1601–1625.

Nagahara H. 1992. Yamato-8002: Partial melting residue on the "unique" chondrite parent body. *Proceedings of the NIPR Symposium on Antarctic Meteorites* 5:191–223.

Nagahara H. and Ozawa K. 1986. Petrology of Yamato-791493, lodranite: Melting, crystallization, cooling history, and relationship to other meteorites. In *The Tenth Symposium on Antarctic Meteorites, Proceedings of the 1985 conference*, edited by Yanai K., Takeda H. and Shimoyama A. Memoirs of the National Institute of Polar Research, Special Issue No. 41. Tokyo: National Institute of Polar Research. pp. 181–205.

Nakamuta Y., Urata K., Shibata Y., and Kuwahara Y. 2017. Effect of $NaCrSi_2O_6$ component on Lindsley's pyroxene thermometer: An evaluation based on strongly metamorphosed LL chondrites. *Meteoritics & Planetary Science* 52:511–521.

Nehru C. E., Weisberg M. K., Boesenberg S., and Kilgore M. 2003. Tafassasset: A metal-rich achondrite with affinities to brachinites (abstract #1370). 34th Lunar and Planetary Science Conference. CD-ROM.

Neumann W., Henke S., Breuer D., Gail H.-P., Schwarz W. H., Trieloff M., Hopp J., and Spohn T. 2018. Modeling the evolution of the parent body of acapulcoites and lodranites: A case study for partially differentiated asteroids. *Icarus* 311:146–169.

Norman M. D., Keil K., Griffin W. L., and Ryan C. G. 1995. Fragments of ancient lunar crust: Petrology and geochemistry of ferroan noritic anorthosites from the Descartes region of the Moon. *Geochimica et Cosmochimica Acta* 59:831–847.

Papike J. J., Spilde M. N., Fowler G. W., Layne G. D., and Shearer C. K. 1995. The Lodran achondrite: Petrogenetic insights from electron and ion microprobe analysis of olivine and orthopyroxene. *Geochimica et Cosmochimica Acta* 59:3051–3070.

Petaev M. I., Barsukova L. D., Lipschutz M. E., Wang M. S., Ariskin A. A., Clayton R. N., and Mayeda T. K. 1994. The Divnoe meteorite: Petrology, chemistry, oxygen isotopes and origin. *Meteoritics & Planetary Science* 29:182–199.

Shearer C. K., Burger P. V., Guan Y., Papike J. J., Sutton S. R., and Atudorei N.-V. 2012. Origin of sulfide replacement textures in lunar breccias. Implications for vapor element transport in the lunar crust. *Geochimica et Cosmochimica Acta* 83:138–158.

Singerling S. A., McCoy T. J., and Gardner-Vandy K. G. 2013. Possible evidence for sulfidization reactions in the miller range brachinites(?) (abstract #1669). 44th Lunar and Planetary Science Conference. CD-ROM.

Singletary S. J. and Grove T. L. 2003. Experimental investigations of ureilite petrogenesis: Relationships between Mg# and smelting event (abstract #1192). 34th Lunar and Planetary Science Conference. CD-ROM.

Skemer P., Katayama I., Jiang Z., and Karato S. 2005. The misorientation index: Development of a new method for calculating the strength of lattice-preferred orientation. *Tectonophysics* 411:157–167.

Starkey N. A., Jackson C. R. M., Greenwood R. C., Parman S., Franchi I. A., Jackson M., Fitton J. G., Stuart F. M.,

Kurz M., and Larsen L. M. 2016. Triple oxygen isotopic composition of high-$^{3}He/^{4}He$ mantle. *Geochimica et Cosmochimica Acta* 176:227–238.

Takeda H., Mori H., Hiroi T., and Saito J. 1994. Mineralogy of new Antarctic achondrites with affinity to Lodran and a model of their evolution in an asteroid. *Meteoritics* 29:830–842.

Warren P. H. and Kallemeyn G. W. 1989. Allan Hills 84025—The second brachinite, far more differentiated than Brachina, and an ultramafic achondritic clast from L chondrite Yamato 75097. Proceedings, 19th Lunar and Planetary Science Conference. pp. 475–486.

Warren P. H. and Rubin A. E. 2012. The Miller Range 090340 dunite: not a uniquely ferroan ureilite, not even a ureilite (abstract #2528). 43rd Lunar and Planetary Science Conference. CD-ROM.

Welten K. C., Nishiizumi K., and Caffee M. W. 2014. Cosmic ray exposure history and pairing of the miller range ungrouped achondrites: MIL 090206, 090340 and 090963 (abstract #2450). 45th Lunar and Planetary Science Conference. CD-ROM.

Wlotzka F. 2005. Cr spinel and chromite as petrogenetic indicators in ordinary chondrites: Equilibration temperatures of petrologic types 3.7 to 6. *Meteoritics & Planetary Science* 40:1673–1702.

Zaslavskaya N. I. and Petaev M. I. 1990. The divnoe meteorite I. Petrology and mineralogy (abstract). 21st Lunar and Planetary Science Conference. p. 1369.